

**OPEN ACCESS**

## LES investigation of infinite staggered wind-turbine arrays

To cite this article: Xiaolei Yang and Fotis Sotiropoulos 2014 *J. Phys.: Conf. Ser.* **555** 012109

View the [article online](#) for updates and enhancements.

### You may also like

- [Wind turbine wake interactions at field scale: An LES study of the SWIFT facility](#)  
Xiaolei Yang, Aaron Boomsma, Matthew Barone et al.
- [Influence of platform dynamic yaw motions on wake, and subsequent impacts on downwind turbine power and loads.](#)  
Marit I Kvittem, Lene Vien Eliassen, Balram Panjwani et al.
- [Study on Numerical Simulation of Wind Turbine](#)  
S Yan, Y T Guo, J Y Zhao et al.



**ECS**  
The  
Electrochemical  
Society  
Advancing solid state &  
electrochemical science & technology

**DISCOVER**  
how sustainability  
intersects with  
electrochemistry & solid  
state science research

# LES investigation of infinite staggered wind-turbine arrays

Xiaolei Yang and Fotis Sotiropoulos<sup>1</sup>

St. Anthony Falls Laboratory, Department of Civil Engineering, University of Minnesota, 2  
Third Avenue SE, Minneapolis, MN 55414, USA

<sup>1</sup> Corresponding author: fotis@umn.edu

**Abstract.** The layouts of turbines affect the turbine wake interactions and thus the wind farm performance. The wake interactions in infinite staggered wind-turbine arrays are investigated and compared with infinite aligned turbine arrays in this paper. From the numerical results we identify three types of wake behaviours, which are significantly different from wakes in aligned wind-turbine arrays. For the first type, each turbine wake interferes with the pair of staggered downstream turbine wakes and the aligned downstream turbine. For the second type, each turbine wake interacts with the first two downstream turbine wakes but does not show significant interference with the second aligned downstream turbine. For the third type, each turbine wake recovers immediately after passing through the gap of the first two downstream turbines and has little interaction with the second downstream turbine wakes. The extracted power density and power efficiency are also studied and compared with aligned wind-turbine arrays.

## 1. Introduction

In wind farms the wakes from upstream turbines affect the power extraction and dynamic loadings of the downstream turbines. This influence depends on the layout of wind turbines, wind directions and many other effects. In comparison with aligned turbine arrays, the turbine wakes are affected by the so-called venturi effects [1] in staggered turbine arrays. The far-wake region of an upstream turbine also interacts with the near wake region of its downstream turbine side by side. How these different wake interactions affect the wake behaviours and power extraction in infinite large staggered wind-turbine arrays will be investigated in this paper using large-eddy simulation with turbines parametrized as actuator disks.

Most previous numerical studies have focused either on wakes of a single stand-alone wind turbine or aligned wind-turbine arrays. For instance, the turbulence characteristics of a single wind turbine wake was studied by Jimenez et al. [2, 3] while turbine spacing effects in infinite aligned wind-turbine arrays were investigated by Calaf et al. [4] and Yang et al. [5]. To the best of our knowledge, the only numerical work on finite staggered wind farms was reported by Ammara et al. [1] by using Reynolds-averaged Navier-Stokes equation with an actuator disk model.

Wind tunnel experiments have also been used to investigate wind turbine wakes. However, it is difficult to mimic infinite large wind-turbine arrays in a wind tunnel experiment because of the limits imposed by the wind tunnel and the inherent side-wall effects. The wake behind a single turbine was investigated by Chamorro and Porté-Agel [6]. Studies on aligned wind-turbine



arrays can be found in the work by Cal et al. [7] and Chamorro and Porté-Agel [8]. Staggered wind-turbines arrays were investigated by Chamorro et al. [9].

## 2. Numerical methods

### 2.1. Governing equations

The LES equations governing the incompressible turbulent flows are the 3D, unsteady, filtered continuity and Navier-Stokes equations. The curvilinear immersed boundary (CURVIB) method [10] is used to solve these equations in order to facilitate future extension of the method to simulate topography effects. In this method the governing equations are first written in Cartesian coordinates  $x_i$  and then transformed fully (both the velocity vector and spatial coordinates are expressed in curvilinear coordinates) in non-orthogonal, generalized, curvilinear coordinates  $\xi^i$ . The transformed equations read in compact tensor notation (repeated indices imply summation) as follows ( $i, j = 1, 2, 3$ ):

$$J \frac{\partial U^j}{\partial \xi^j} = 0, \quad (1)$$

$$\begin{aligned} \frac{1}{J} \frac{\partial U^i}{\partial t} = & \frac{\xi_l^i}{J} \left( -\frac{\partial}{\partial \xi^j} (U^j u_l) + \frac{\mu}{\rho} \frac{\partial}{\partial \xi^j} \left( \frac{g^{jk}}{J} \frac{\partial u_l}{\partial \xi^k} \right) \right. \\ & \left. - \frac{1}{\rho} \frac{\partial}{\partial \xi^j} \left( \frac{\xi_l^j p}{J} \right) - \frac{1}{\rho} \frac{\partial \tau_{lj}}{\partial \xi^j} + f_i \right), \end{aligned} \quad (2)$$

where  $\xi_l^i = \partial \xi^i / \partial x_l$  are the transformation metrics,  $J$  is the Jacobian of the geometric transformation,  $u_i$  is the  $i^{th}$  component of the velocity vector in Cartesian coordinates,  $U^i = (\xi_m^i / J) u_m$  is the contravariant volume flux,  $g^{jk} = \xi_l^j \xi_l^k$  are the components of the contravariant metric tensor,  $\rho$  is the density,  $\mu$  is the dynamic viscosity,  $p$  is the pressure,  $f_i$  ( $i = 1, 2, 3$ ) are the body forces introduced by the wind turbines and  $\tau_{ij}$  represents the anisotropic part of the subgrid scale stress tensor, which is modelled by the eddy-viscosity subgrid scale model [11]. For details of the CURVIB method and numerical schemes, please refer to the papers [10, 12].

### 2.2. Actuator disk model

In the actuator disk model a wind turbine rotor is represented by a permeable circular disk that is discretized using an unstructured triangular grid. Drag forces exerted by the turbine rotor on wind are uniformly distributed over the disk surface to model the momentum extraction by a turbine rotor. The thrust force on the wind turbine rotor is calculated from the following expression

$$F_T = \frac{1}{2} \rho C_T U_\infty^2 \frac{\pi}{4} D^2, \quad (3)$$

where  $\rho$  is the air density,  $C_T$  is the thrust coefficient,  $U_\infty$  is the incoming velocity and  $D$  is the diameter of wind turbine rotor. In the present work, the  $C_T$  is determined from the one-dimensional momentum theory [13] and reads as

$$C_T = 4a(1 - a), \quad (4)$$

where  $a$  is the axial induction factor of the turbine rotor, which is specified in our simulations. The incoming velocity  $U_\infty$  for a wind turbine in an infinite wind-turbine array is calculated using the relation from one-dimensional momentum theory:

$$U_\infty = u_d / (1 - a). \quad (5)$$

In the above equation  $u_d$  is the disk-averaged streamwise velocity on the actuator disk.

Generally, the positions of grid nodes of the actuator disk do not coincide with those of the background (fluid) domain. Quantities are transferred between the two grids through discrete delta functions. The velocities on the disk are interpolated from the background grid by:

$$u_i(\mathbf{X}) = \sum_{g_f} u_i(\mathbf{x}) \delta_h(\mathbf{x} - \mathbf{X}) V(\mathbf{x}), \quad (6)$$

where  $\mathbf{x}$  and  $\mathbf{X}$  denote the coordinates of the meshes for fluid and actuator disks, respectively,  $g_f$  represents the collection of background grid cells,  $\delta_h$  is the discrete delta function and  $V(\mathbf{x})$  is the volume of the background cell. The forces on the background grid nodes are distributed from the grid nodes of actuator disks by the expression shown as follows:

$$f_i(\mathbf{x}) = \sum_{g_t} f_i(\mathbf{X}) \delta_h(\mathbf{x} - \mathbf{X}) A(\mathbf{X}), \quad (7)$$

where  $g_t$  represents the collection of actuator disk cells and  $A(\mathbf{X})$  is the area of actuator disk cell. In the present work a smoothed discrete delta function proposed by Yang et al. [14] was used.

### 2.3. Boundary conditions

In all simulations, periodic boundary conditions are used in the horizontal directions. A free-slip boundary condition is used at the top boundary and a wall model is used at the bottom boundary. A mean pressure gradient is applied in the streamwise direction to ensure a constant mass flow rate. At the bottom boundary, the shear stress boundary condition and no-flux boundary condition are used for the wall-parallel and wall-normal velocity components, respectively. The wall shear stress is calculated from the logarithmic law for rough wall [15], which is given as follows:

$$\frac{U}{u_*} = \frac{1}{\kappa} \ln \frac{z}{z_{0,lo}}, \quad (8)$$

where  $U$  is the mean wall-parallel velocity and  $z_{0,lo}$  is the roughness height of the land surface. In the present work, the magnitude of the instantaneous parallel velocity  $U_2$  at the second off-wall grid node is used for calculating  $u_*$  from the Eq (8), which is calculated as follows:

$$U_2 = \sqrt{u_2^2 + v_2^2}, \quad (9)$$

where  $u_2$  and  $v_2$  are the instantaneous streamwise and spanwise velocity components at the second off-wall grid node, respectively.

## 3. Numerical results

Four infinite staggered wind-turbine arrays together with two infinite aligned arrays are simulated to study the effects of turbine layout and spacing on the wake behaviour and power extraction of infinite wind farms. In all cases, the area of the land is fixed and is set equal to  $30D$  and  $20D$  in the streamwise and spanwise directions, respectively. For the staggered cases, the number of rows of wind turbines in the streamwise direction ( $N_{t,x}$ ) is fixed at 4. The number of turbines in each row ( $N_{t,y}$ ) is varied to be 3, 4, 5 and 6 for the four staggered cases, respectively. The simulated layout of a staggered wind farm is demonstrated in Figure 1, which shows a specific layout with 4 rows of wind turbine in the streamwise direction and 5 turbines in each row. The two aligned wind farm cases are simulated in order to compare with the corresponding staggered case with 5 turbines in each row. The two aligned cases consist of: 1)

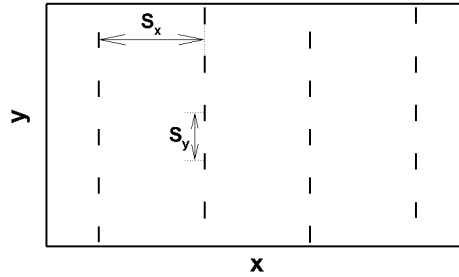


Figure 1: Schematic of staggered wind-turbine array. The turbines are represented by solid segments and  $S_x$  and  $S_y$  denote the turbine spacings in streamwise and spanwise directions, respectively.

4 rows in the streamwise direction with 5 turbines in each row; and 2) 2 rows with 10 turbines in each row. For all cases, the hub height of the wind turbine  $z_h = D$  and the domain size in the vertical direction  $H = 10D$ . The computational grid consists of 200, 150 and 128 grid nodes in the streamwise, spanwise and vertical directions, respectively. The effect of viscous terms is neglected because of the very high Reynolds number of the atmospheric boundary layer. The roughness height of the land  $z_{0,lo} = 10^{-4}H$ . The induction factor  $a = 0.25$ . In the following discussions, we will denote the sets of cases by “S  $N_{t,x}$ - $N_{t,y}$ ” and “A  $N_{t,x}$ - $N_{t,y}$ ” for staggered and aligned layouts, respectively.

In order to facilitate the physical interpretation of our results, the velocity field is normalized by the equivalent geostrophic velocity  $G$ , which is calculated from the geostrophic drag law [16],

$$\frac{G}{u_*} = \sqrt{A^2 + \left( \frac{1}{\kappa} \ln \frac{u_*}{f z_{0,hi}} - C \right)^2}, \quad (10)$$

where the Coriolis parameter  $f = 2\Omega \sin \theta$  is set equal to  $1 \times 10^{-4} s^{-1}$  (where  $\Omega$  is the angular speed of the earth and latitude  $\theta = 40^\circ$ ),  $A = 11.25$ ,  $C = 4.5$ , and  $z_{0,hi}$  is the effective roughness height of the wind farm covered land. The total friction velocity  $u_*$  in the above equation is provided by LES and the effective roughness height is calculated by using the mean streamwise velocity at  $z = 0.175H$  via Eq. (8).

In Figure 2, we show the contours of instantaneous streamwise velocity on the x-y plane positioned at hub height. As seen, the flow fields for all cases exhibit high speed streaks, low speed wakes and wake meandering. While at first glance the general behaviour of staggered and aligned wakes are nearly the same, significant differences are observed in the structure of the high speed streaks. For the case A4-5 the high speed streaks are elongated spanning the entire gap between adjacent columns of turbines. For the case A2-10, however, the high speed streaks are only located within the gaps between turbine columns in the near wake and merge with each other in the far wake. The high speed streaks behave significantly different for the staggered cases in which the high speed streaks usually cross different columns of turbines and slow down locally because of the momentum extraction by turbines.

Figure 3 shows the mean flow field for each case, averaged in time and in space (every 2 staggered turbines for staggered arrays and every turbine for aligned arrays). For staggered arrays we observe three different types of wake behavior. For the first type, each turbine wake interferes with the pair of staggered downstream turbine wakes and the aligned downstream turbine (Figures 3a and 3b). For the second type, each turbine wake interacts with the first two downstream turbine wakes but does not show significant interference with the second aligned downstream turbine (Figure 3c). For the third type (Figure 3d), each turbine wake recovers

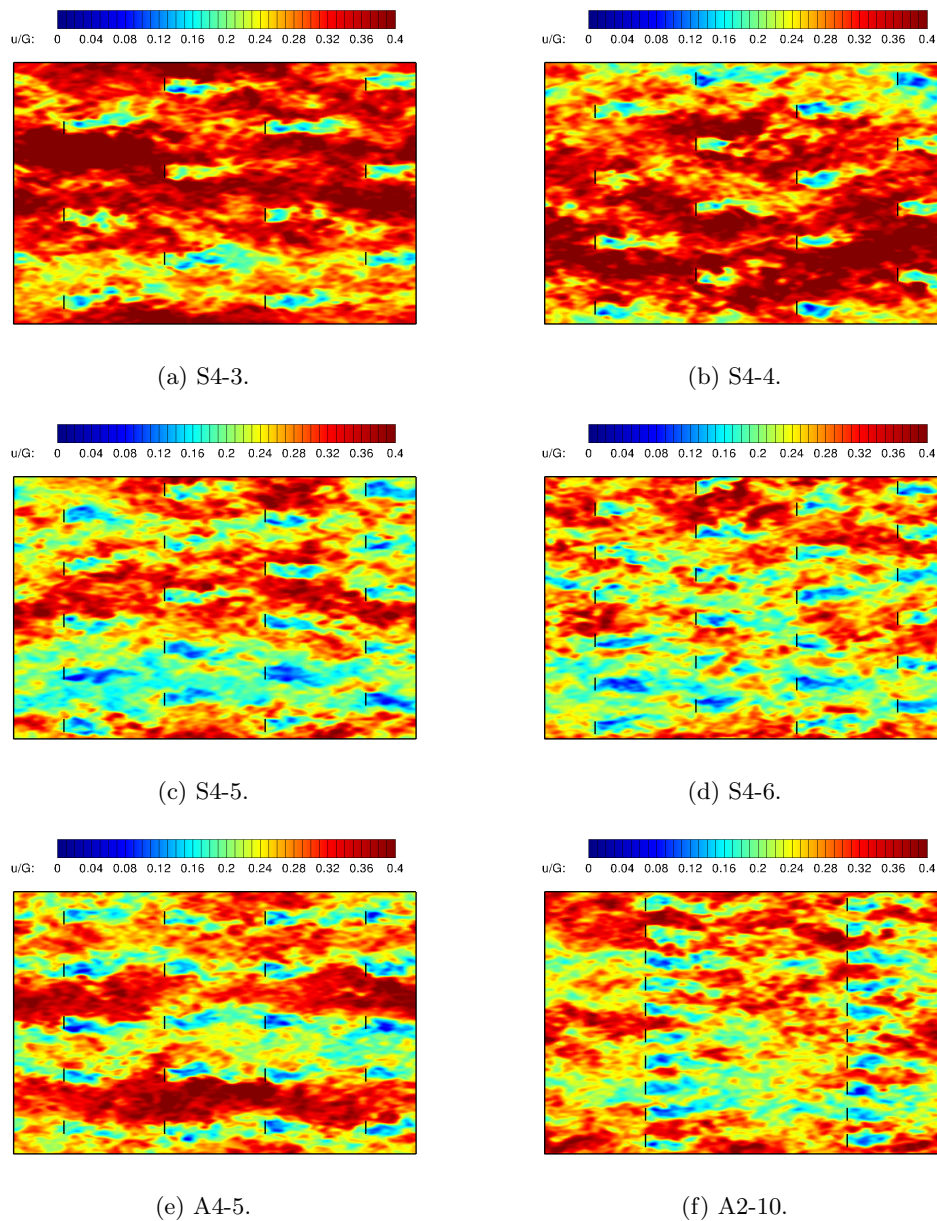


Figure 2: Contours of instantaneous streamwise velocity on the x-y plane at the hub height normalized by  $G$  for staggered (a through d) and aligned (e and f) wind farms.

immediately after passing through the gap of the first two downstream turbines and has little interaction with the second downstream turbine wakes. Comparing the wakes for the S4-5 and A4-5 and A2-10 cases, we observe that the wake recovery is more significant for the S4-5 and A2-10 layouts before the wake encounters the next row of immediately downstream wind turbines. However, the mechanism for wake recovery is quite different. For the A2-10 layout, the wake recovers only because of the streamwise turbine spacing. For the S4-5 layout, however, there are two factors affecting wake recovery: the streamwise turbine spacing and the acceleration effect caused by the first two downstream turbines, an effect which increases with decreasing the spanwise turbine spacing for current cases.

In Figure 4, we show the mean streamwise velocity profiles averaged in time and horizontal

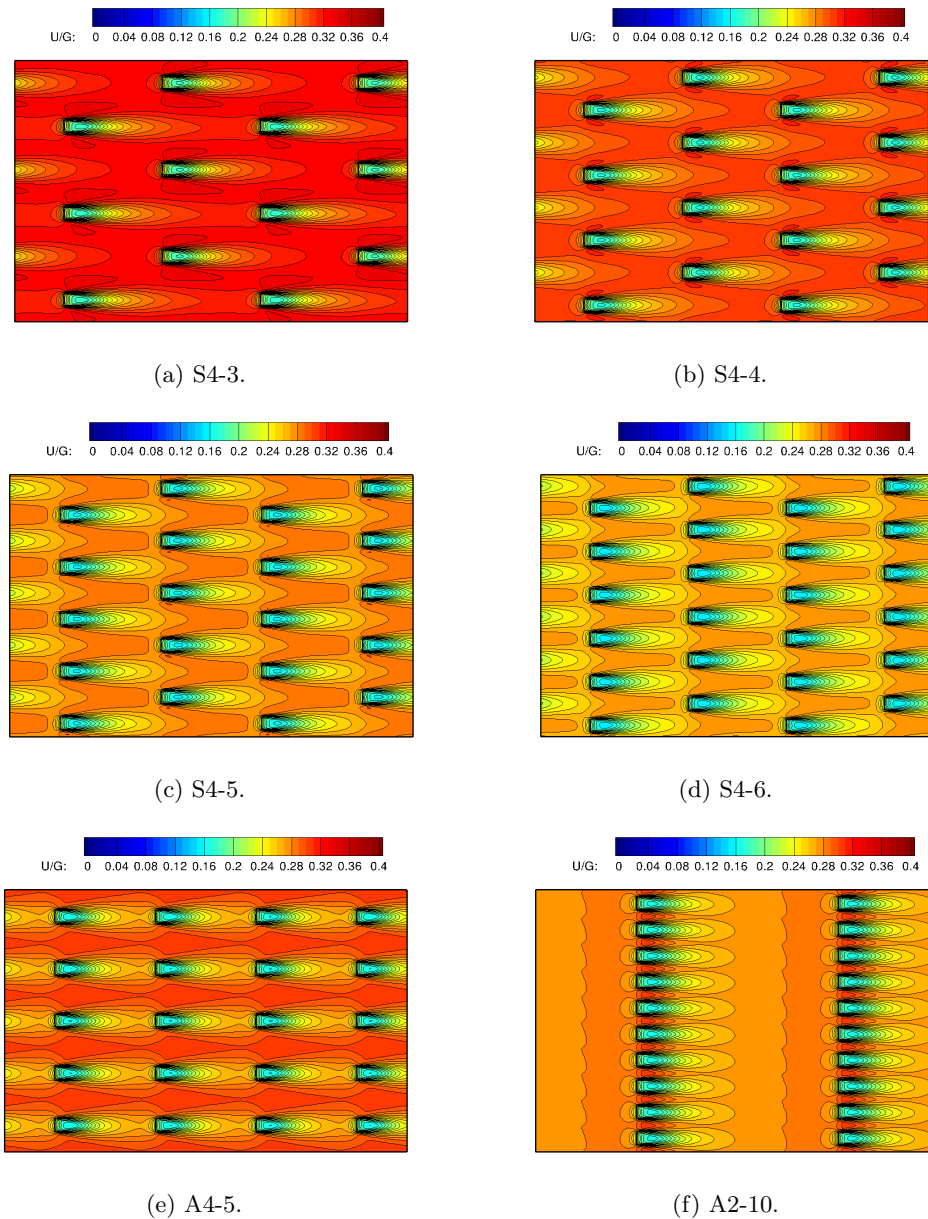


Figure 3: Contours of mean streamwise velocity on the x-y plane at the hub height normalized by  $G$  for staggered (a through d) and aligned (e and f) wind farms.

directions. As seen in Figure 4a, the two logarithmic layers known to form for aligned wind farms (Calaf et al. [4], Yang et al. [5]) also exist for the staggered wind farms. In Figure 4b, we compare mean velocity profiles for staggered and aligned cases. It is seen that the three profiles are nearly collapsed with each other for the outer logarithmic layer ( $z > z_h$ ). For the inner part, the profile from case A4-5 is shifted upwards compared to the profiles from the other two cases, which are nearly identical in the lower part.

Let finally investigate the effect of turbine spacing on the extracted power. Figure 5a shows the extracted power density for all simulated cases as a function of  $N_t$  ( $N_t = N_{t,x} \times N_{t,y}$ ), which

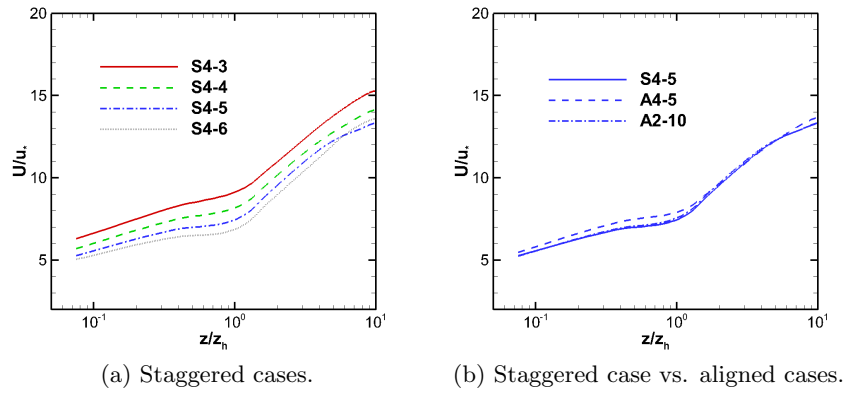


Figure 4: Mean streamwise velocity profiles.

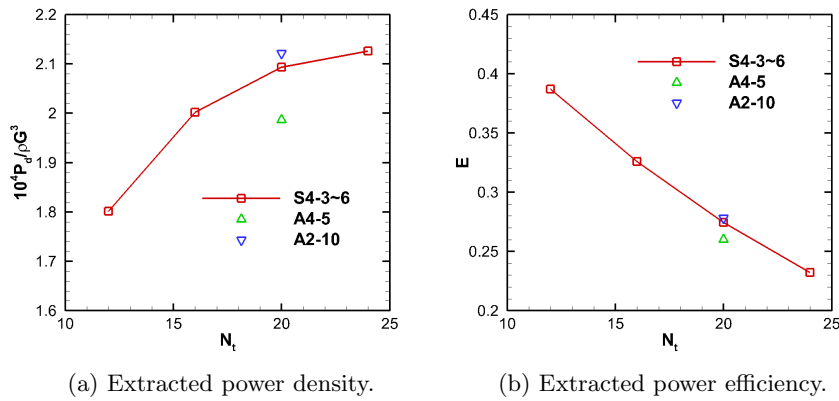


Figure 5: Extracted power density and power efficiency.

is defined as follows:

$$P_d \equiv \frac{P}{S_x S_y}, \quad (11)$$

where  $P$  is the extracted power averaged over all turbines. It is seen that the extracted power density increases with increasing the number of turbines. For the same number of wind turbine ( $N_t = 20$ ), the case A2-10 is able to extract somewhat higher power density than that from the staggered case S4-5. While the case A4-5 gives much lower power density than the corresponding staggered case. Figure 5b shows the extracted power efficiency, which is defined as follows:

$$E \equiv P/P_{1tb}, \quad (12)$$

where  $P_{1tb}$  is the power that would be extracted from a single stand-alone wind turbine under the same geostrophic wind speed and land surface roughness. It is seen that the extracted power efficiency decreases with increasing the number of turbines in each row. Similar to the power density, the efficiency from the cases A2-10 and A4-5 is somewhat higher and lower, respectively, than that for the S4-5 case.

#### 4. Summary

In this paper, we investigate the wake behaviour of infinite staggered wind-turbine arrays by carrying out four cases with different spanwise turbine spacings at the same streamwise turbine spacing together with the other two aligned cases. In aligned turbine arrays, the wake recovery mainly depends on the size of the streamwise turbine spacing. In staggered turbine arrays, acceleration (venturi) effect caused by the first two downstream turbines also plays an important role in wake recovery besides of the streamwise turbine spacing. Based on how one turbine wake interacts with its downstream turbine wakes, three different wake patterns are identified for staggered turbine arrays.

For a given turbine occupied area, staggered turbine layout is preferred for locations without a fixed prevailing wind direction. An aligned turbine array with a longer streamwise turbine spacing, on the other hand, is suitable for locations with a fixed prevailing wind direction.

#### Acknowledgments

This work was supported by Department of Energy DOE (DE-EE0002980) and Xcel Energy through the Renewable Development Fund (grant RD3-42). Computational resources were provided by the University of Minnesota Supercomputing Institute.

#### References

- [1] Ammara I, Leclerc C and Masson C 2002 *J. Sol. Energy Eng.* **124** 345–356
- [2] Jimenez A, Crespo A, Migoya E and Garcia J 2007 *Journal of Physics: Conference Series* **75** 012041
- [3] Jimenez A, Crespo A, Migoya E and Garcia J 2008 *Environ. Res. Lett.* **3** 015004
- [4] Calaf M, Meneveau C and Meyers J 2010 *Phys. Fluids* **22** 015110
- [5] Yang X, Kang S and Sotiropoulos F 2012 *Physics of Fluids (1994-present)* **24** 115107
- [6] Chamorro L P and Porté-Agel F 2009 *Boundary-Layer Meteorol.* **132** 129–149
- [7] Cal R B, Lebrón J, Castillo L, Kang H S and Meneveau C 2010 *J. Renewable Sustainable Energy* **2** 013106
- [8] Chamorro L P and Porté-Agel F 2011 *Energies* **4** 1–22
- [9] Chamorro L P, Arndt R E A and Sotiropoulos F 2011 *Boundary-Layer Meteorol.*
- [10] Ge L and Sotiropoulos F 2007 *J. Comput. Phys.* **225** 1782–1809
- [11] Germano M, Piomelli U, Moin P and Cabot W H 1991 *Phys. Fluids A* **3** 1760–1765
- [12] Kang S, Lightbody A, Hill C and Sotiropoulos F 2011 *Adv. Water Resour.* **34** 98–113
- [13] Hansen M O L 2000 *Aerodynamics of wind turbines* (James & James (Science Publishers) Ltd)
- [14] Yang X, Zhang X, Li Z and He G W 2009 *J. Comput. Phys.* **228** 7821–7836
- [15] Jiménez J 2004 *Annu. Rev. Fluid Mech.* **36** 173–196
- [16] Tennekes H and Lumley J L 1972 *A First Course in Turbulence* (MIT Press, Cambridge, MA)